# Bond length-bond angle correlation in densified silica—Results from $^{17}$O NMR spectroscopy

Nicole M. Trease,[1] Ted M. Clark,[1] Philip J. Grandinetti,[1,a)] Jonathan F. Stebbins,[2,b)] and Sabyasachi Sen[3,c)]
[1]*Department of Chemistry, Ohio State University, 100 West 18th Avenue, Columbus, Ohio 43210-1106, USA*
[2]*School of Earth Sciences, Stanford University, Stanford, California 94305-2115, USA*
[3]*Department of Materials Science and Engineering, University of California, Davis, California 95616-5270, USA*

(Received 28 January 2017; accepted 24 April 2017; published online 11 May 2017)

Pressure induced correlated evolution of the distributions of the Si–O distance and Si–O–Si inter-tetrahedral bond angle in vitreous silica quenched from pressures of up to ~14 GPa at ambient temperature is measured in unprecedented detail using two-dimensional dynamic-angle-spinning $^{17}$O nuclear magnetic resonance spectroscopy. The results demonstrate that, in contrast to the conventional wisdom, vitreous silica undergoes irreversible structural changes even at pressures as low as ~8 GPa. These structural changes at the short range involve a progressive reduction in the mean Si–O–Si angle and a broadening of the corresponding distribution, with increasing pressure. This bond angle reduction is accompanied by a concomitant monotonic increase in the mean Si–O distance. The mean values of the Si–O–Si angle and Si–O distance at various pressures closely follow the minimum in the corresponding potential energy surface calculated for the $H_6Si_2O_7$ dimer molecule. *Published by AIP Publishing.* [http://dx.doi.org/10.1063/1.4983041]

## I. INTRODUCTION

Vitreous silica ($SiO_2$) has fundamental importance as an archetypal glass former with diverse technological applications,[1] and its structure-property relations have been studied intensively for decades using both experiments and simulations.[2–21] Significant controversy, however, exists in the literature regarding the structure of a vitreous silica network at the intermediate-range and its response to pressure. Since Bridgman's work in the middle of the last century,[22] it is well known that silica can undergo permanent densification at ambient temperature upon compression above 10 GPa. It is also widely believed that pressure induced changes up to ~10 GPa are reversible upon unloading.[12] Although an increase in the Si coordination number is widely accepted to be primarily responsible for the densification of silica at pressures above 20 GPa, the structural mechanism for densification at lower pressures remains somewhat unclear. The only consensus in this respect is the observation of a pressure-induced reduction of the mean Si–O–Si bond angle between corner-shared $SiO_4$ tetrahedra that may serve as an important mechanism of compression of the network at pressures below 10 GPa. On the basis of an *in situ* high-pressure vibrational spectroscopic study, Hemley and co-workers[10] proposed a concomitant narrowing of the Si–O–Si bond angle distribution (BAD) and an increase in the relative fraction of 3- and 4-membered rings at the expense of more open or larger rings. On the other hand, in a careful *in situ* Raman spectroscopic study, Poe *et al.*[13] proposed a narrowing of the mean Si–O–Si angle and the BAD and a corresponding lengthening of mean Si–O bond distance, but no change in ring size distribution up to 8 GPa at 700 °C where the glass density increased by ~6%. These authors reported an absence of any Si–O bond lengthening induced by Si–O–Si angle reduction, at least up to 2 GPa. On the other hand, in an earlier study, Walrafen and Krishnan[23] reported insignificant change in the Raman spectra of vitreous silica up to 9 GPa at ambient temperature where the glass density increased by ~8%. The corresponding structural change was attributed at ambient temperature to intermediate-range length scale (beyond next-nearest neighbors) to reconcile the differences between two studies. These results demonstrate that the density and structure are not uniquely related in the glassy state.[12]

Besides experimental studies, extensive molecular dynamics simulations have been carried out by Dove, Trachenko, and co-workers[16,24,25] and Huang and Kieffer[26–28] to elucidate the effect of pressure on the structure of vitreous silica in the low pressure regime. Dove, Trachenko, and co-workers developed a structural model of compression of silica within the framework of a rigid-unit-mode (RUM) model, recognizing that the energy associated with the deformation of $SiO_4$ tetrahedra is much higher than the energy required for the rotation of these tetrahedra about a common vertex. According to these authors, at low pressures up to ~3 GPa, silica is compressible without the need to break the tetrahedral topology. However, beyond such pressures, defective (non-ideal) structures begin to appear such that the breakdown of intermediate-range order begins at pressures ~5 GPa and coordination number begins to change significantly. These structural changes are predicted to be partially recoverable

a)Electronic mail: grandinetti.1@osu.edu
b)Electronic mail: stebbins@stanford.edu
c)Electronic mail: sbsen@ucdavis.edu

upon decompression. In contrast, a rather different description of pressure-induced changes in vitreous silica glass was proposed on the basis of classical molecular dynamics simulations by Huang and Kieffer.[26–28] These authors observed pressure-induced localized reversible structural changes in silica that are facilitated by Si–O bond rotations around the Si–Si axis and a decrease in the Si–O bond angle. However, no significant change in Si–O distances was observed. This reversible densification process does not involve the breaking or formation of any bonds and the ring size distribution remained practically unchanged, even at pressures up to 15-20 GPa. Therefore further studies are clearly needed to build a fundamental atomistic understanding of the pressure-induced densification process of the open tetrahedral structural network of vitreous silica.

Recent studies have shown that $^{17}$O dynamic-angle-spinning nuclear magnetic resonance (DAS NMR) spectroscopy[29–32] is capable of providing a direct measurement of the Si–O–Si bond angle and Si–O bond distance distributions as well as insights into any correlation between these structural parameters.[33,34] Here we report the results of a $^{17}$O DAS NMR study of the structure of vitreous silica samples quenched from two different pressures, ~8 GPa and ~13.5 GPa at ambient temperature. The results are compared with those obtained on a sample of vitreous silica prepared at ambient pressure, to investigate the pressure-induced changes in the distributions of the Si–O–Si bond angle, Si–O and Si–Si distances in the network, and their mechanistic connection with densification.

## II. EXPERIMENTAL

### A. Sample preparation

The $^{17}$O-enriched vitreous silica was synthesized via typical melt quenching route. First, a sample of $^{17}$O-enriched silica gel was synthesized by hydrolysis of $SiCl_4$ with 77% $^{17}$O enriched $H_2O$ in diethyl ether. After drying, approximately 500 mg gel was heated at 1825 °C for 3 h in pure Ar in a Pt–Rh crucible and then cooled in air to prepare the glass. This sample was coarsely crushed and one portion (sample S-1) was reserved. The remaining sample was divided into two halves and compressed at ambient temperature in a high pressure multi-anvil apparatus at Bayerische Geoinstitut (Bayreuth, Germany) to maximum pressures of 8.0 ± 1.5 GPa and 13.5 ± 1.5 GPa. Pressure was subsequently lowered to obtain densified glass samples. These samples are designated as S-2 and S-3, respectively, in the subsequent discussion. Because we synthesized the isotopically enriched glass, rather than machining a solid billet of commercial optical-grade glass, our high pressure glass samples were loaded into the apparatus in a coarsely granular form, and recovered in a highly fragmented form. This precluded high-precision density measurements on recovered samples.

### B. $^{17}$O NMR

At 9.4 T, the $^{17}$O DAS NMR experiments were performed on a Chemagnetics CMX II spectrometer using a modified

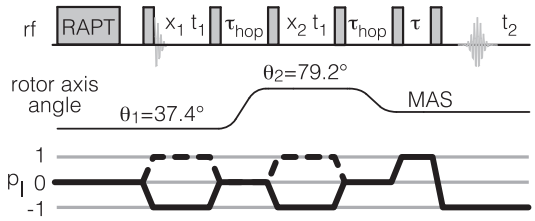


FIG. 1. The FSG-RAPT enhanced shifted-echo MAS-detected dynamic-angle spinning sequence.

version of a homebuilt 4 mm DAS probe that was previously reported.[35] All measurements were performed at ambient pressure several months after the samples were prepared. The shifted-echo magic-angle-spinning-(MAS)-detected DAS pulse sequence[36] was used with a Frequency-Switched Gaussian (FSG)–Rotor Assisted Population Transfer (RAPT)[37] preparation period to enhance the central transition polarization as illustrated in Fig. 1. Sample rotation rate was ~15 kHz. The DAS angle pair (37.38°, 79.19°) where $x_1 = x_2 = 0.5$ was employed in removing the second-order anisotropic broadenings, and detection was carried out at 54.74° to eliminate all chemical shift anisotropy contributions to the anisotropic line shape. The optimized FSG-RAPT parameters used were $\nu_{off}$ = ±49 000 kHz, loop counter = 400, and the Gaussian pulse width was 14 $\mu$s ($\sigma$ = 2.4 $\mu$s). A recycle delay of 40 s was used for all $^{17}$O NMR experiments, and the chemical shift data are referenced with respect to $^{17}$O in tap water.

At 14.1 T, the $^{17}$O and $^{29}$Si MAS NMR measurements were performed on a Varian Inova spectrometer and a Varian/Chemagnetics 3.2 mm probe and sample spinning frequencies of 18 kHz. Frequencies were referenced to 20% $^{17}$O $H_2O$ and to tetramethylsilane, respectively. For both nuclides, single-pulse acquisition was used with a radiofrequency tip angle (solids) of about 30°, corresponding to pulse widths of 1.1 ($^{29}$Si) and 0.35 ($^{17}$O) $\mu$s. Recycle delays of 10 s were chosen to optimize signal-to-noise; no differential relaxation was detected with longer delays.

### C. Correlating NMR parameters to structure

For interpreting the structure of silicate glasses and describing the Si–O–Si angle distribution, the most important $^{17}$O NMR parameter is the quadrupolar asymmetry parameter, $\eta_q$. A dependence of $\eta_q$ on the Si–O–Si angle as related to the fractional s character of the bridging oxygen has been known for some time.[31,38,39] In addition to the quadrupolar asymmetry parameter, the quadrupolar coupling constant, $C_q$, is another NMR parameter determined by the electric field gradient at bridging oxygen sites and is dependent on structural features in the first coordination sphere, especially the Si–O distance and Si–O–Si angle.[40] The distance dependence of $C_q$ is negative, i.e., for a fixed Si–O–Si angle, the $C_q$ parameter increases in magnitude and becomes more negative as the average Si–O distance increases. Clark and Grandinetti[41] developed parameterized relationships for both $\eta_q$ and the quadrupolar coupling constant, $C_q$, given by

$$\eta_q(\Omega) = b\left(\frac{1}{2} - \frac{\cos\Omega}{\cos\Omega - 1}\right)^{\beta} \quad (1)$$

and

$$C_q(d_{\mathrm{TO}}, \Omega) = a\left(\frac{1}{2} + \frac{\cos\Omega}{\cos\Omega - 1}\right)^{\alpha} + m_d\left(d_{\mathrm{TO}} - d^{\circ}_{\mathrm{TO}}\right), \quad (2)$$

where $\Omega$ is the Si–O–Si bond angle. The values of $b = 4.73$ and $\beta = 1.12$ for $\eta_q$ and $a = -6.53$ MHz, $\alpha = 1.80$, $m_d = -12.86$ MHz/Å, and $d^{\circ}_{\mathrm{TO}} = 1.654$ Å for $C_q$ were obtained by fitting the experimental or calculated results of ferrierite, cristobalite, quartz, and coesite.[41]

As reported previously,[33,41] the simultaneous measurement of $C_q$ and $\eta_q$ can be used in combination with Eqs. (1) and (2) to obtain the correlation between the Si–O–Si bond angle, Si–O distance, and Si–Si next-nearest neighbor distance in the structure of vitreous silica. Here, the same approach is taken to calculate these structural parameters in vitreous silica quenched from different pressures.

## III. RESULTS AND DISCUSSION

### A. $^{29}$Si NMR results

$^{29}$Si MAS spectra for glasses from all three pressures are approximately Gaussian in shape (Fig. 2), as has typically been reported for ambient pressure silica glasses.[42] For ambient pressure, 8, and 13.5 GPa, respectively, the center of gravity of the $^{29}$Si NMR peak is located at −110.7, −108.9, and −106.7 ppm while the values of the full width at half maximum (FWHM) are 11.6, 13.3, and 15.2 ppm. Long acquisitions for the highest pressure glass detected no clear signals near −150 ppm or −190 ppm,[43] as would be expected for $SiO_5$ or $SiO_6$ groups, with a detection limit of about 0.5%. We note that in that previous study, higher quality $^{29}$Si MAS data on a $^{29}$Si-enriched silica glass quenched from a melt at 6 GPa also showed no detectable $SiO_5$, in contrast to spectra for alkali silicate glasses subjected to similar pressures, in which this species and $SiO_6$ groups were readily detectable at concentrations of several percent.

A number of empirical correlations between the mean Si–O–Si bond angle and $^{29}$Si chemical shift in framework silicates, including silica polymorphs, have been summarized.[42] These typically predict a variation of about 1.6°/ppm in shift, corresponding to a narrowing of the mean Si–O–Si angle by about 6.5° in our comparison of the ambient with the 13.5 GPa glass. Moreover, the monotonically increasing FWHM of the $^{29}$Si NMR peak with pressure (Fig. 2) suggests a concomitant broadening in the bond angle distribution. Of course, $^{29}$Si chemical shifts are expected to vary with other local structural parameters, making a unique interpretation of these results difficult.

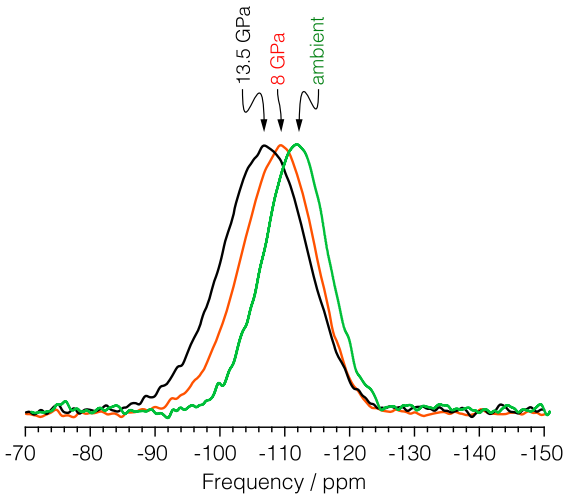


FIG. 2. $^{29}$Si MAS spectra for glasses from all three pressures.

### B. $^{17}$O NMR results

The experimental $^{17}$O 2D DAS spectra along with experimental MAS cross sections for all three silica samples are shown in Fig. 3. Spectra were modeled using a previously reported[33] algorithm that performs two linear least squares analyses. In the first, each $\omega_1$ cross section is fit for $C_q$ and an area, assuming it contains a single site, with fixed constraints of Gaussian broadening, total isotropic shift ($\omega_1 = \delta_{iso} = \delta_{CS} + \delta_q$), and a linear relationship between $C_q$ and $\eta_q$. The second fits the 2D spectra as a whole, where Gaussian broadening and the slope and intercept of the linear relationship between $C_q$ and $\eta_q$ are varied. The best fit 2D simulated DAS spectra along with the residuals between the fitted simulation and experimental spectra for all three samples are also shown in Fig. 3. While this model is able to provide a satisfactory fit to the experimental data, it makes an over simplified assumption that each $\omega_1$ (anisotropic) cross section contains a single site. In reality, each $\omega_1$ cross section contains overlapping line shapes arising from a multitude of sites with varying $C_q$, $\eta_q$, and $\delta_{CS}$ values. By modeling each cross section with a single site, our analysis effectively determines the mean $C_q$ and $\eta_q$ of each cross section. This biases the overall $C_q$ and $\eta_q$ distributions obtained from the full 2D spectrum towards smaller widths, and as a result smaller distribution widths in the Si–O–Si angle and Si–O distance. Implementing a more accurate model, however, would require additional assumptions about the form of the NMR parameter distribution associated with each $\omega_1$ cross section. With this understanding, we expect the correlations and the modes of the distributions obtained with this approach to be accurate with the caveat that the distribution widths reflect, at best, the lower limits of the true widths. We do not expect this model analysis to limit comparisons across samples.

Three-dimensional correlations between the NMR parameters, $C_q$, $\eta_q$, and $\delta_{CS}$, were extracted from the fitted data in Fig. 3 to investigate the nature of the pressure induced structural changes. In Fig. 4 are 2D histograms along with corresponding 1D projections showing the correlations of (a) $C_q$ and $\eta_q$, (b) $C_q$ and $\delta_{CS}$, and (c) $\eta_q$ and $\delta_{CS}$ for the three samples. Statistical distributions of the $^{17}$O NMR parameters derived from the fitted data are provided in Table I. Comparison of the NMR parameters for the ambient sample with those reported in a previous study by Clark *et al.*[33] show no difference within the uncertainty of the measurement for the $C_q$ and $\eta_q$ parameters, although the $\delta_{CS}$ data are systematically shifted to slightly larger values in this study. For all three samples, the chemical shift data are consistent with oxygen coordinated by two tetrahedrally coordinated silicon.[44] The $C_q$ versus $\eta_q$ correlation is much stronger for the glass when compared with $SiO_2$ polymorphs, and the slope of the correlation is steeper.

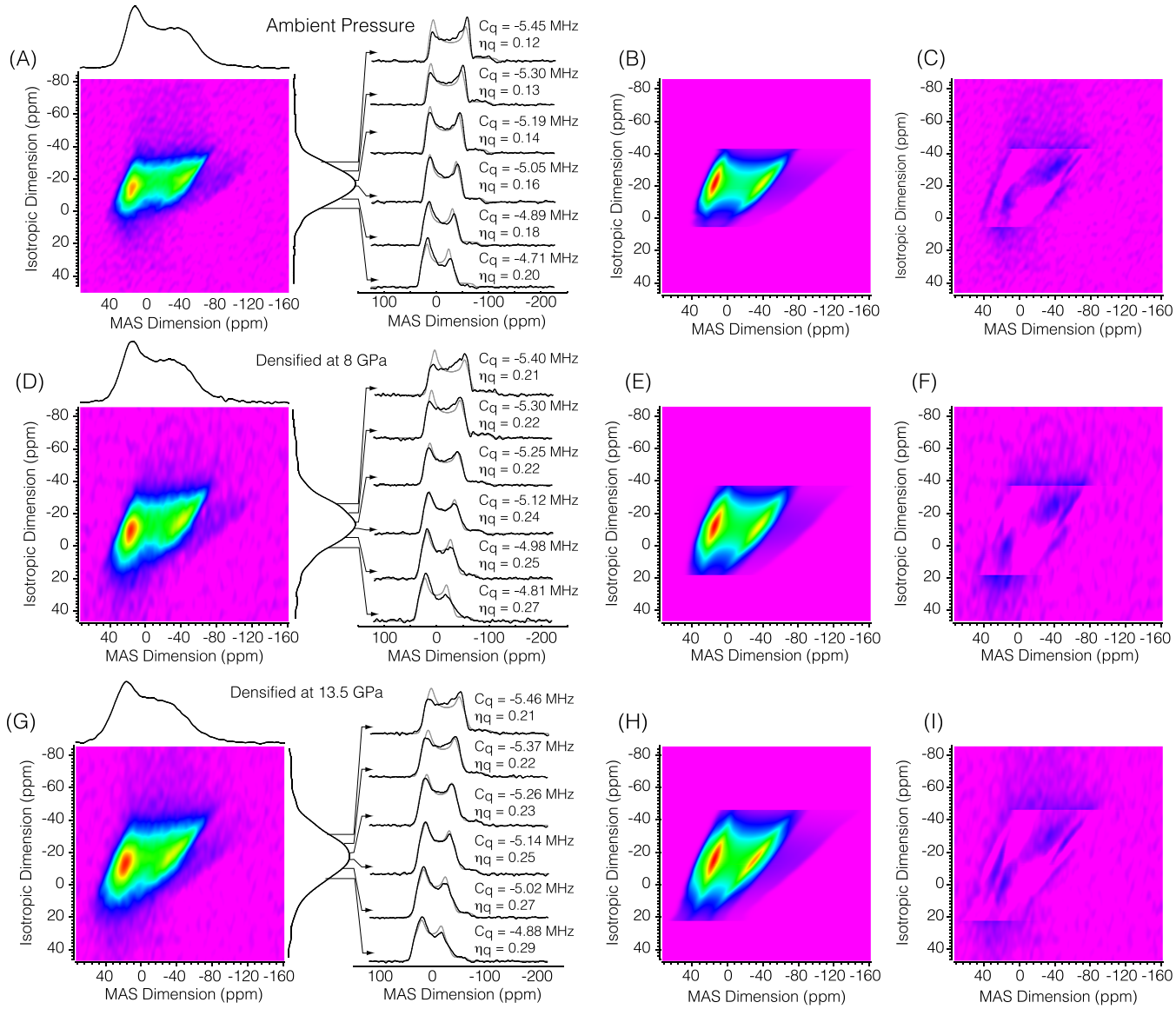


FIG. 3. DAS spectra for $SiO_2$ glass at ambient pressure ((a)–(c)), densified at 8 GPa ((d)–(f)), and densified at 13.5 GPa ((g)–(i)) $SiO_2$ glass at 9.4 T. ((a), (d), and (g)) The experimental 2D DAS spectra along with 1D projections onto the MAS and isotropic dimensions, experimental MAS cross sections and their best fit simulations (gray) are also shown. ((b), (e), and (h)) The best fit 2D simulated DAS spectra. ((c), (f), and (i)) The residuals between the fitted simulations and experimental spectra.

Also, a large number of oxygen sites in these glass samples have $C_q$ values between −4.0 and −5.0 MHz, while it is rare for bridging the oxygen site in crystalline $SiO_2$ to have a $C_q$ value smaller in magnitude than −5.0 MHz. To the best of our knowledge, the prevalence of oxygen sites with small $|C_q|$ values is an important characteristic that has not been accounted for in simulated models of silica glass. For example, the $C_q$ values calculated for silica glass generated by classical molecular dynamics simulations agree more closely with the values for $SiO_2$ polymorphs than with the values reported here for silica glass.[45]

Visual inspection of both the isotropic and MAS dimensions of the $^{17}O$ 2D NMR spectra indicates that systematic changes occur as a function of applied pressure, e.g., with increasing pressure the width of the 1D projection onto the isotropic dimension axis increases (Fig. 3). With increasing pressure, $\eta_q$ systematically shifts to larger values (Fig. 4(b)). Since the Si–O–Si bond angle increases as $\eta_q$ decreases, the trend observed in Fig. 4(b) implies a corresponding reduction in the Si–O–Si bond angle with increasing pressure. It is interesting to note that the $^{17}O$ $\eta_q$ parameter of the majority of crystalline $SiO_2$ polymorphs has $\eta_q \leq 0.25$. The same observation can be made for the $\eta_q$ values for the silica sample S-1 prepared at ambient pressure. This result suggests that the frequency of small Si–O–Si bond angles in silica glass does not diverge greatly from the frequency of such angles in crystalline $SiO_2$. The shifting of $\eta_q$ to significantly higher values for the compressed samples, however, suggests that small Si–O–Si bond angles become much more prevalent in these samples than in the crystalline $SiO_2$ polymorphs. A comparison of the $^{17}O$ NMR parameters in Table I indicates that $\eta_q$ is significantly more responsive to pressure-induced changes in the structure than $C_q$ or chemical shift.

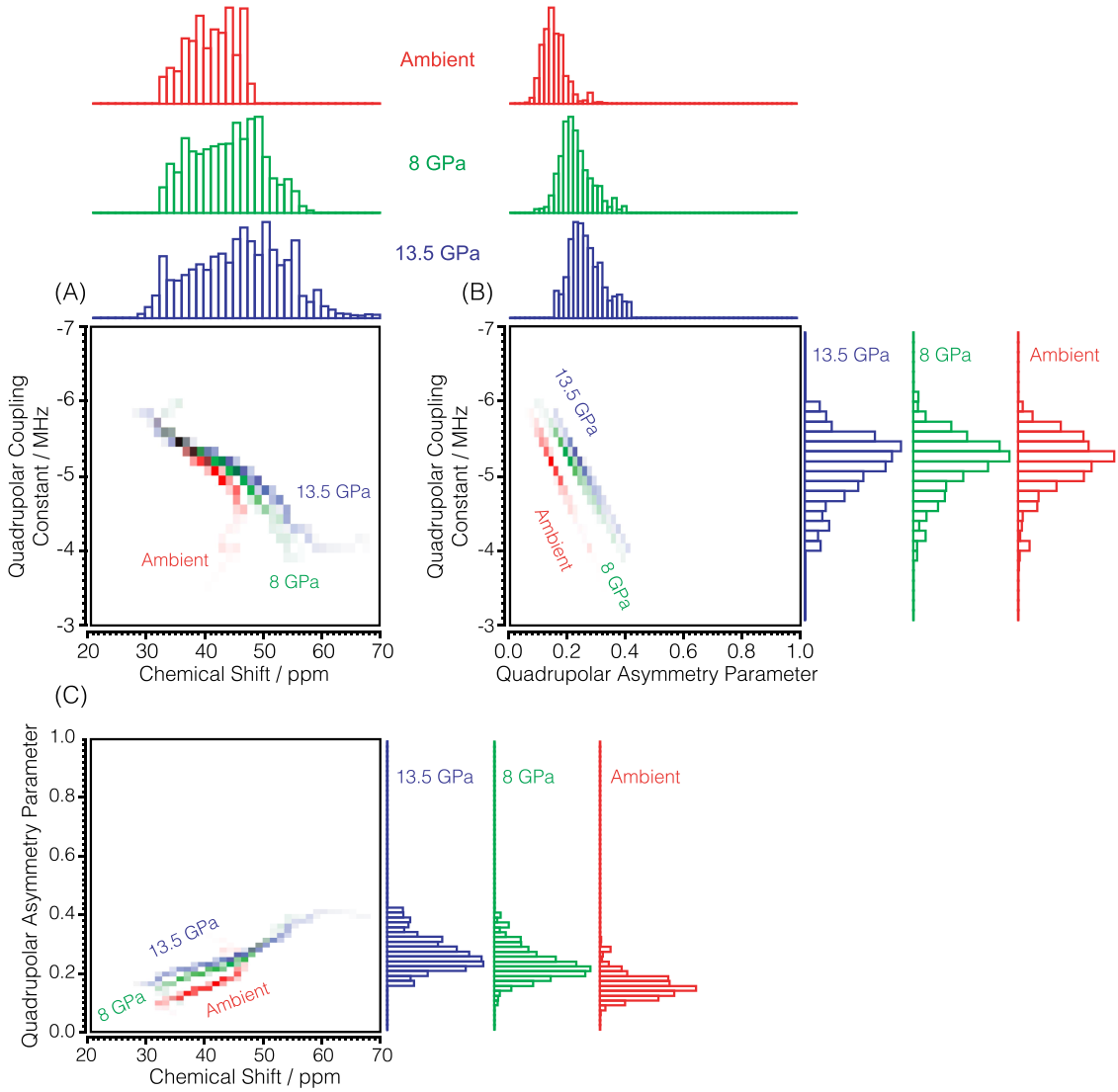


FIG. 4. Two-dimensional correlations of the NMR parameters, (a) $C_q$ and $\delta_{CS}$, (b) $C_q$ and $\eta_q$, and (c) $\eta_q$ and $\delta_{CS}$, are given for ambient $SiO_2$ (red), $SiO_2$ densified at 8 GPa (green), and $SiO_2$ densified at 13.5 GPa (blue). The 2D histograms along with corresponding 1D projections were extracted from the 2D spectra in Fig. 3. Also shown in (a) is a grid of lines (gray) obtained from Eqs. (1) and (2) by varying the Si–O distance with the Si–O–Si angle held constant and the Si–O–Si angle with the Si–O distance held constant.

### C. Structural parameters and mechanism of densification

The experimental two-dimensional histograms of $C_q$ and $\eta_q$ are mapped into the two-dimensional histograms of the Si–O–Si angle versus distance using Eqs. (1) and (2) and are shown in Fig. 5(a). The two-dimensional histograms of the Si–O distance and Si–O–Si angle versus Si–Si distance are then obtained using a law-of-cosines calculation (Figs. 5(b) and 5(c)). The corresponding one-dimensional projections are

TABLE I. Statistical parameters describing the distribution of NMR parameters calculated from measured one-dimensional distributions in ambient $SiO_2$ glass and $SiO_2$ glass densified at both 8 GPa and 13.5 GPa.

| | | Mean | Mode | Median | Std. dev. | Skew | Kurtosis |
|---|---|---|---|---|---|---|---|
| $C_q$ | Ambient | −5.12 MHz | −5.20 MHz | −5.18 MHz | 0.375 MHz | 0.977 | 1.575 |
| | 8 GPa | −5.10 MHz | −5.20 MHz | −5.18 MHz | 0.394 MHz | 0.672 | 0.443 |
| | 13.5 GPa | −5.06 MHz | −5.33 MHz | −5.14 MHz | 0.427 MHz | 0.575 | −0.135 |
| $\eta_q$ | Ambient | 0.152 | 0.142 | 0.146 | 0.0408 | 0.977 | 1.575 |
| | 8 GPa | 0.226 | 0.208 | 0.215 | 0.0551 | 0.672 | 0.443 |
| | 13.5 GPa | 0.261 | 0.225 | 0.251 | 0.0589 | 0.575 | −0.135 |
| $\delta_{CS}$ | Ambient | 40.02 ppm | 43.13 ppm | 40.21 ppm | 4.06 ppm | −0.221 | −0.961 |
| | 8 GPa | 42.95 ppm | 48.13 ppm | 43.26 ppm | 5.87 ppm | −0.007 | −0.883 |
| | 13.5 GPa | 44.99 ppm | 49.38 ppm | 45.13 ppm | 7.84 ppm | 0.023 | −0.516 |

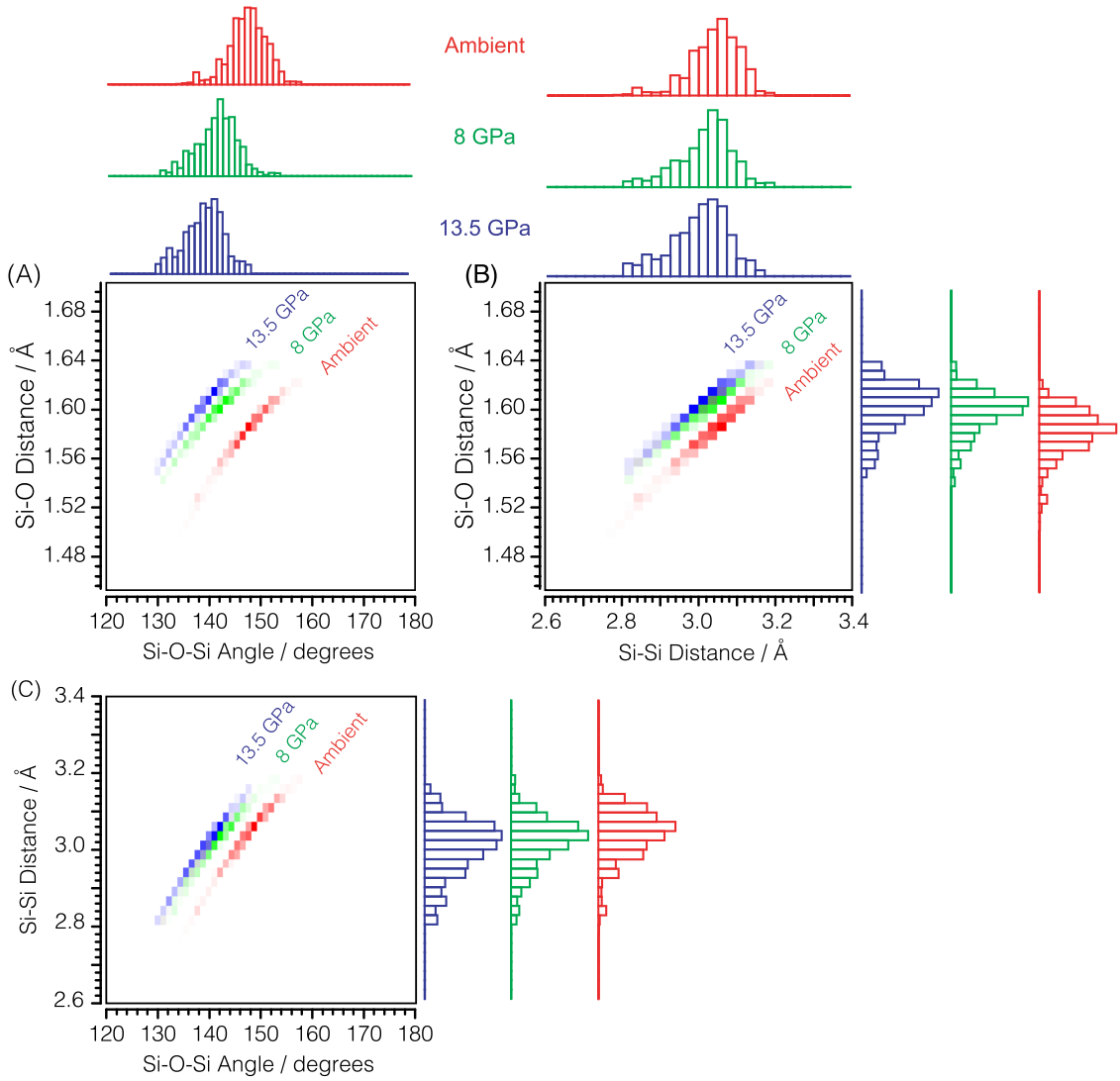


FIG. 5. Two-dimensional histograms of bridging oxygen structural parameters, (a) Si–O–Si angle versus Si–O distance, (b) Si–O distance versus Si–Si distance, and (c) Si–O–Si angle versus Si–Si distance, derived from NMR parameter distributions in Fig. 4 using Eqs. (1) and (2) for ambient $SiO_2$ (red), $SiO_2$ densified at 8 GPa (green), and $SiO_2$ densified at 13.5 GPa (blue). Statistical parameters calculated from both the NMR and structural 1D histograms are given in Table II.

shown in Fig. 6, and the statistical parameters summarizing these distributions are included in Table II.

First, we focus on the distribution of the structural parameters in the vitreous silica sample prepared at ambient pressure. The Si–O–Si bond angle distribution shown in Fig. 6 peaks (mode) at 147.7° with a standard deviation of 3.8°. This peak position is in agreement, within the precision of the experiment, with previous $^{17}O$ DAS NMR[33] measurements and with high-energy X-ray and neutron diffraction studies.[7,46] The 1D Si–O distance distribution has a mode of 1.586 Å with a standard deviation of 0.020 Å which is in agreement with previous $^{17}O$ NMR results,[33] although it is somewhat lower than 1.605 Å obtained by diffraction methods.[47] It should be noted that the Si–O–Si bond angle and the Si–O and Si–Si distance distributions are constructed in this study through model assumptions, which may account for the observed deviations in peak position and the width of the distribution, compared to those obtained in previous diffraction studies. The 1D Si–Si distance distribution has a mode of 3.061 Å and a standard deviation of 0.067 Å, in reasonable agreement with the previous study.[33] The experimentally measured two-dimen sional structural distributions (Fig. 5) exhibit strong, nearly linear correlations among the Si–O–Si angle, Si–O distance, and Si–Si distance for all three samples. The correlations for sample S-1 are in good agreement with those reported earlier for a different but similarly prepared sample,[33] and an unintuitive positive correlation between the Si–O distance and Si–O–Si angle is observed here once again, this time for all three samples. However, the most prominent effect of pressure on the glass structure is apparent in the correlation between the Si–O distance and the Si–O–Si angle which, while having a similar slope, is shifted to smaller Si–O–Si angles for samples S-2 and S-3 prepared at high pressure compared to the ambient pressure S-1 sample. The mean Si–O–Si angle decreases from 147.7° to 138.8° while the mean Si–O distance increases from 1.583 Å to 1.603 Å monotonically with increasing pressure, although the width of the distribution of these structural parameters does not change significantly (Table II). This reduction in the mean bond angle is roughly consistent with that inferred above from the 1D $^{29}Si$ spectra, although

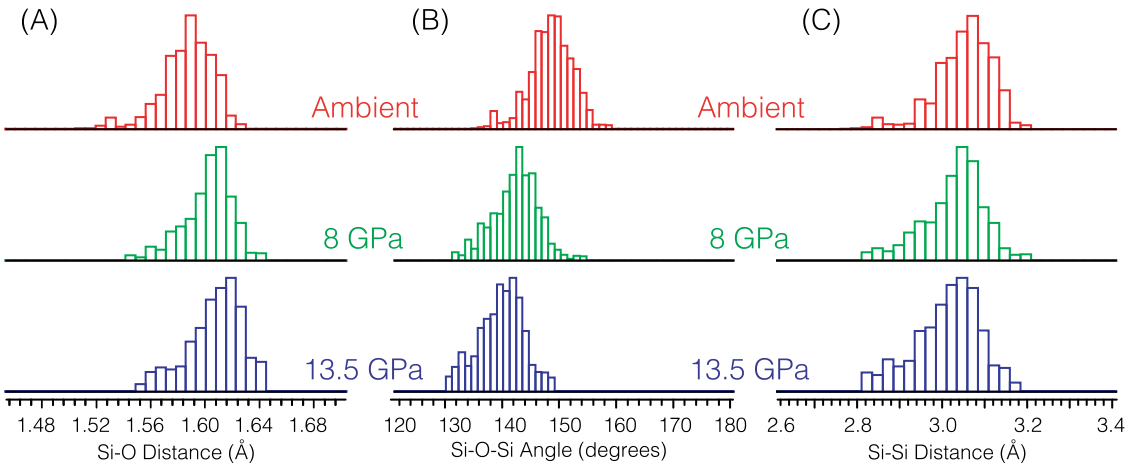


FIG. 6. One-dimensional structural histograms of (a) Si–O distance, (b) Si–O–Si bond angle, and (c) Si–Si distance for silica glass at ambient pressure (red), densified at 8 GPa (green), and densified at 13.5 GPa (blue). It can be seen that as the densification of $SiO_2$ occurs at increasing pressures the mean Si–O distance increases, the mean Si–O–Si bond angle decreases and the mean Si–Si distance remains relatively unchanged.

somewhat greater in magnitude. However, because the $^{17}O$ DAS experiment appears to better separate effects of the bond angle and distance, we consider these results a better measure of this predominant structural change with pressure. Moreover, a comparison of the two-dimensional structural distributions indicates that the structure of the sample decompressed from 8 GPa (S-2) is more similar to the sample decompressed from 13.5 GPa (S-3) than it is to the uncompressed sample (S-1). These results, when taken together, clearly indicate that (i) vitreous silica undergoes irreversible structural changes even at ~8 GPa, and (ii) the densification process in this pressure regime and at ambient temperature primarily involves Si–O–Si bond angle reduction and concomitant lengthening of the Si–O bonds.

Typically significant densification is reported only above 10 GPa, although more recently Deschamps *et al.*[12] showed that significant recoverable densification starts near 10 GPa. We are not, however, claiming to see structural changes without recovered densification. It is more likely that there is relatively small recovered densification or the pressures in all these studies are too uncertain. There are often large uncertainties in pressures in multi-anvil experiments, both ours and previous and we have been generous with the error bars accordingly. Nonetheless, $^{17}O$ DAS is clearly sensitive enough to detect such subtle structural changes even when recoverable densification is low or undetectable.

The most probable Si–O–Si bond angles determined here are in very close agreement with values determined in a molecular dynamics simulation for silica glass at pressures of 8 GPa and 15 GPa, and values reported for densified silica glass.[26–28,48,49] The shift towards smaller Si–O–Si angles at higher pressures has been interpreted in the past as indicative of the presence of smaller ring sizes in densified silica.[50] However, more recent molecular dynamics simulations[27] have reported quite the opposite finding where, at high pressure, smaller rings dissolve in favor of larger rings. Therefore, the observation of a pressure-induced lowering of the mean Si–O–Si angle in the present study cannot be attributed *a priori* to the formation of smaller rings. Moreover, a change in the ring statistics would involve Si–O bond breaking and switching events at a minimum, which would be difficult to activate at ambient temperature. On the contrary, it is tempting to argue that the ring size statistics in these samples remains largely unchanged. In this case, the reduction in the mean Si–O–Si angle with pressure may involve puckering of the rings in the tetrahedral network.

Interestingly, the Si–O–Si bond angle distributions for all samples do not extend below 130°. This is most apparent for sample S-3 in which the number of oxygen sites with

TABLE II. Statistical parameters describing the structure calculated from measured one-dimensional distributions in ambient $SiO_2$ glass and $SiO_2$ glass densified at both 8 GPa and 15 GPa.

| Parameter | | Mean | Mode | Median | Std. dev. | Skew | Kurtosis |
|---|---|---|---|---|---|---|---|
| Ω | Ambient | 147.7° | 147.7° | 148.0° | 3.8° | −0.42 | 0.50 |
| | 8 GPa | 141.4° | 142.1° | 142.0° | 4.1° | −0.20 | 0.22 |
| | 13.5 GPa | 138.8° | 140.9° | 139.3° | 4.0° | −0.24 | −0.34 |
| *d*(Si–O) | Ambient | 1.58 Å | 1.59 Å | 1.59 Å | 0.02 Å | −1.02 | 1.69 |
| | 8 GPa | 1.60 Å | 1.61 Å | 1.60 Å | 0.02 Å | −0.72 | 0.51 |
| | 13.5 GPa | 1.60 Å | 1.62 Å | 1.61 Å | 0.02 Å | −0.61 | −0.09 |
| *d*(Si–Si) | Ambient | 3.04 Å | 3.061 Å | 3.05Å | 0.07 Å | −0.88 | 1.32 |
| | 8 GPa | 3.02 Å | 3.04 Å | 3.03 Å | 0.07 Å | −0.58 | 0.33 |
| | 13.5 GPa | 3.00 Å | 3.04 Å | 3.01 Å | 0.08 Å | −0.50 | −0.21 |

Si–O–Si angles between 130° and 135° is significantly increased relative to samples S-1 and S-2, and yet the angle distribution sharply terminates at 130°. An asymmetric Si–O–Si bond angle distribution was proposed quite early for silica glass,[51] and the existence of a lower threshold value for Si–O–Si angles may be indicative of steric constraints. A minimum Si–O–Si angle of ~130° would preclude 2-membered rings but is consistent with the presence of 3- or 4- membered rings in the glass structure.[52] The concomitant increase in the Si–O distance with the lowering of the Si–O–Si angle under compression is presumably driven by the energetics of the Coulombic repulsion between Si–Si next-nearest neighbors that maintain the modal value of the Si–Si distance nearly constant in all samples (Table II), irrespective of pressure.

Further insight into the structural mechanism of densification can be gained via a comparison between the pressure dependent variation in the correlated distribution of the Si–O distance and Si–O–Si angle in these glasses with the potential energy surface defined by these two structural variables in crystalline $SiO_2$ polymorphs and in $H_6Si_2O_7$ dimer molecules, as obtained on the basis of *ab initio* calculations.[53] This comparison is shown in Fig. 7. The shallow minimum (valley) in the potential energy surface of crystalline $SiO_2$ and $H_6Si_2O_7$ dimers is defined by a rather weak but decidedly negative correlation between the Si–O distance and Si–O–Si angle. The pressure dependent variation in the mean values of these two structural parameters in vitreous silica, as obtained in the present study, clearly follows this negative correlation well (Fig. 7). Finally, it is interesting to note that the kurtosis of the Si–O–Si bond angle distribution progressively decreases and becomes negative with increasing pressure, implying a flatter distribution at higher pressure (Table II). This trend is consistent with a corresponding widening of the valley in the potential energy surface in Fig. 7.

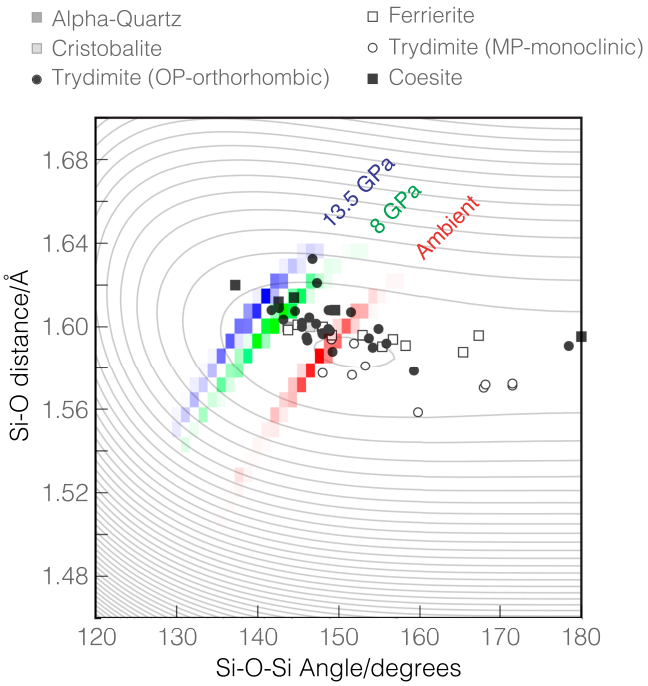


FIG. 7. Si–O–Si vs. Si–O distribution in vitreous silica samples S-1 (red), S-2 (green), and S-3 (blue). The contours correspond to the potential energy surface of $H_6Si_2O_7$ dimers calculated using restricted Hartree-Fock with a 6-311+G(2d,p) basis set using Gaussian 03.[54] The symbols indicate the Si–O distances and Si–O–Si angles of all known crystalline polymorphs of $SiO_2$.

## IV. CONCLUSIONS

The onset and nature of the pressure induced permanent structural changes in vitreous silica have remained controversial to date. We have utilized $^{17}O$ DAS NMR spectroscopy to obtain three-dimensional histograms correlating the $^{17}O$ chemical shift, quadrupolar coupling constant, and quadrupolar coupling asymmetry parameter for the bridging oxygen sites in vitreous silica quenched from pressures up to ~13.5 GPa, at ambient temperature. Using existing correlations between NMR parameters and local structure, the distribution in the quadrupolar coupling parameters is mapped into two dimensional histograms correlating the Si–O–Si angle and Si–O and Si–Si distances. These results demonstrate that at ambient temperature the lower limit of pressure for the onset of structural changes that persist after decompression in vitreous silica is ~8 GPa. A comparison between the quenched structures up to ~13.5 GPa suggests no significant change in the Si coordination and ring size distribution. Instead, the corner-shared tetrahedral network undergoes a decrease in the average Si–O–Si angle and Si–Si distance and a concomitant increase in the Si–O distance, which suggest a compression and possible puckering of the constituent rings. Contrary to intuition, these structural changes are not elastically recoverable upon decompression as the resulting networks all evolve along the locus of the minima in the Si–O–Si versus Si–O potential energy surface.

## SUPPLEMENTARY MATERIAL

See supplementary material for the additional NMR characterization of the three silica samples and the Gaussian 03 input file for generating the potential energy surface of the $H_6Si_2O_7$ dimer shown in Fig. 7.

## ACKNOWLEDGMENTS

This material is based upon work supported in part by the National Science Foundation under Grant No. CHE-1506870. We thank Jeffrey A. Allwardt (then at Stanford University) for the densification experiments on the silica glass, done using the facilities of the Bayerisches Geoinstitut, Universitt Bayreuth, Germany and supported by NSF Grant No. EAR-0408410 to J.F.S. S.S. acknowledges support from NSF Grant No. DMR1505185.

[1]T. Uchino, J. Ceram. Soc. Jpn. **113**, 17 (2005).
[2]Q. Mei, C. J. Benmore, S. Sen, R. Sharma, and J. L. Yarger, Phys. Rev. B **78**, 144204 (2008).
[3]V. Inamura, Y. Katayama, and W. Utsumi, J. Phys.: Condens. Matter **19**, 415104 (2007).
[4]Y. Katayama and Y. Inamura, Nucl. Instrum. Methods Phys. Res., Sect. B **238**, 154 (2005).
[5]S. Susman, K. J. Volin, D. L. Price, M. Grimsditch, J. P. Rino, R. K. Kalia, P. Vashishta, G. Gwanmesia, Y. Wang, and R. C. Libermann, Phys. Rev. B **43**, 1194 (1991).
[6]C. Z. Tan and J. Arndt, J. Non-Cryst. Solids **249**, 47 (1999).

[7]J. Neuefeind and K.-D. Liss, Bunsen-Ges. Phys. Chem. Chem. Phys. **100**, 1341 (1996).
[8]A. Hiramatsu, M. Arai, H. Shibazaki, M. Tsunekawa, T. Otomo, A. Hannon, S. Bennington, N. Kitamura, and A. Onodera, Physica B **219-220**, 287 (1996).
[9]W. J. Malfait, W. E. Halter, and R. Verel, Chem. Geol. **256**, 269 (2008).
[10]R. J. Hemley, H. K. Mao, P. M. Bell, and B. O. Mysen, Phys. Rev. Lett. **57**, 747 (1986).
[11]L. Giacomazzi and A. Pasquarello, J. Phys.: Condens. Matter **19**, 415112 (2007).
[12]T. Deschamps, J. Margueritat, C. Martinet, A. Mermet, and B. Champagnon, Sci. Rep. **4**, 7193 (2014).
[13]B. T. Poe, C. Romano, and G. Henderson, J. Non-Cryst. Solids **341**, 162 (2004).
[14]X. Yuan and A. N. Cormack, J. Non-Cryst. Solids **319**, 31 (2003).
[15]Y. Xianglong and A. N. Cormack, J. Non-Cryst. Solids **283**, 69 (2001).
[16]K. Trachenko and M. T. Dove, Phys. Rev. B **67**, 064107 (2003).
[17]L. P. Davila, M.-J. Caturla, A. Kubota, B. Sadigh, T. D. de la Rubia, J. F. Shackelford, S. H. Risbud, and S. H. Garofalini, Phys. Rev. Lett. **91**, 205501 (2003).
[18]W. Jin, R. K. Kalia, P. Vashishta, and J. P. Rino, Phys. Rev. B **50**, 118 (1994).
[19]J. Lacks, Phys. Rev. Lett. **80**, 5385 (1998).
[20]S. Kohara and K. Suzuya, J. Phys.: Condens. Matter **17**, S77 (2005).
[21]M. G. Tucker, D. A. Keen, and K. Trachenko, J. Phys.: Condens. Matter **17**, S67 (2005).
[22]P. W. Bridgman, Am. J. Sci. **237**, 7 (1939).
[23]G. E. Walrafen and P. N. Krishnan, J. Chem. Phys. **74**, 5328 (1981).
[24]K. Trachenko and M. T. Dove, J. Phys.: Condens. Matter **14**, 7449 (2002).
[25]K. Trachenko, M. T. Dove, V. Brazhkin, and F. S. El'kin, Phys. Rev. Lett. **93**, 135502 (2004).
[26]L. Huang and J. Kieffer, Phys. Rev. B **69**, 224203 (2004).
[27]L. Huang, L. Duffrene, and J. Kieffer, J. Non-Cryst. Solids **349**, 1 (2004).
[28]L. Huang and J. Kieffer, Phys. Rev. B **69**, 224204 (2004).
[29]A. Llor and J. Virlet, Chem. Phys. Lett. **152**, 248 (1988).
[30]B. F. Chmelka, K. T. Mueller, A. Pines, J. F. Stebbins, Y. Wu, and J. W. Zwanziger, Nature **339**, 42 (1989).
[31]I. Farnan, P. J. Grandinetti, J. H. Baltisberger, J. F. Stebbins, U. Werner, M. A. Eastman, and A. Pines, Nature **358**, 31 (1992).
[32]P. J. Grandinetti, J. T. Ash, and N. M. Trease, Prog. Nucl. Magn. Reson. Spectrosc. **59**, 121 (2011).
[33]T. M. Clark, P. J. Grandinetti, P. Florian, and J. F. Stebbins, Phys. Rev. B **70**, 064202 (2004).
[34]T. Charpentier, P. Kroll, and F. Mauri, J. Phys. Chem. C **113**, 7917 (2009).
[35]M. A. Eastman, P. J. Grandinetti, Y. K. Lee, and A. Pines, J. Magn. Reson. **98**, 333 (1992).
[36]P. J. Grandinetti, J. H. Baltisberger, U. Werner, A. Pines, I. Farnan, and J. F. Stebbins, J. Phys. Chem. **99**, 12341 (1995).
[37]S. Prasad, H. T. Kwak, T. Clark, and P. J. Grandinetti, J. Am. Chem. Soc. **124**, 4964 (2002).
[38]A. E. Geissberger and P. J. Bray, J. Non-Cryst. Solids **54**, 121 (1983).
[39]U. Sternberg, Solid State Nucl. Magn. Reson. **2**, 181 (1993).
[40]T. M. Clark and P. J. Grandinetti, Solid State Nucl. Magn. Reson. **16**, 55 (2000).
[41]T. M. Clark and P. J. Grandinetti, J. Phys.: Condens. Matter **15**, S2387 (2003).
[42]K. J. D. Mackenzie and M. E. Smith, *Multinuclear Solid-State NMR of Inorganic Materials* (Pergamon, 2002).
[43]X. Xue, J. F. Stebbins, M. Kanzaki, P. F. McMillan, and B. Poe, Am. Mineral. **76**, 8 (1991).
[44]X. Xue, J. F. Stebbins, and M. Kanzaki, Am. Mineral. **79**, 31 (1994).
[45]S. Sen, C. A. Russell, and T. Mukerji, Phys. Rev. B **72**, 174205 (2005).
[46]H. Poulsen, J. Neuefeind, H.-B. Neumann, J. Schneider, and M. Zeidler, J. Non-Cryst. Solids **188**, 63 (1995).
[47]A. Wright, J. Non-Cryst. Solids **179**, 84 (1994).
[48]R. A. B. Devine, R. Dupree, I. Farnan, and J. J. Capponi, Phys. Rev. B **35**, 2560 (1987).
[49]R. G. D. Valle and E. Venuti, Phys. Rev. B **54**, 3809 (1996).
[50]J. P. Rino, I. Ebbsjö, R. K. Kalia, A. Nakano, and P. Vashishta, Phys. Rev. B **47**, 3053 (1993).
[51]R. L. Mozzi and B. E. Warren, J. Appl. Cryst. **2**, 164 (1969).
[52]T. Uchino, Y. Kitagawa, and T. Yoko, Phys. Rev. B **61**, 234 (2000).
[53]G. Gibbs, A. Wallace, D. Cox, R. Downs, N. Ross, and K. Rosso, Am. Mineral. **94**, 1085 (2009).
[54]M. J. Frisch, G. W. Trucks, H. B. Schlegel, G. E. Scuseria, M. A. Robb, J. R. Cheeseman, J. A. Montgomery, T. Vreven, K. N. Kudin, J. C. Burant, J. M. Millam, S. S. Iyengar, J. Tomasi, V. Barone, B. Mennucci, M. Cossi, G. Scalmani, N. Rega, G. A. Petersson, H. Nakatsuji, M. Hada, M. Ehara, K. Toyota, R. Fukuda, J. Hasegawa, M. Ishida, T. Nakajima, Y. Honda, O. Kitao, H. Nakai, M. Klene, X. Li, J. E. Knox, H. P. Hratchian, J. B. Cross, V. Bakken, C. Adamo, J. Jaramillo, R. Gomperts, R. E. Stratmann, O. Yazyev, A. J. Austin, R. Cammi, C. Pomelli, J. W. Ochterski, P. Y. Ayala, K. Morokuma, G. A. Voth, P. Salvador, J. J. Dannenberg, V. G. Zakrzewski, S. Dapprich, A. D. Daniels, M. C. Strain, O. Farkas, D. K. Malick, A. D. Rabuck, K. Raghavachari, J. B. Foresman, J. V. Ortiz, Q. Cui, A. G. Baboul, S. Clifford, J. Cioslowski, B. B. Stefanov, G. Liu, A. Liashenko, P. Piskorz, I. Komaromi, R. L. Martin, D. J. Fox, T. Keith, M. A. Al-Laham, C. Y. Peng, A. Nanayakkara, M. Challacombe, P. M. W. Gill, B. Johnson, W. Chen, M. W. Wong, C. Gonzalez, and J. A. Pople, GAUSSIAN 03, Revision E.01, Gaussian, Inc., 2003.